

## Correlation between earthquake intensity parameters and damage indices of high-rise RC chimneys

Yikun Qiu, Changdong Zhou<sup>\*</sup>, Siha A

School of Civil Engineering, Beijing Jiaotong University, Beijing, China

### ARTICLE INFO

#### Keywords:

Chimneys  
Correlation  
Ground motion parameter  
Structural damage  
Period elongation effect  
Higher modes effect

### ABSTRACT

This present paper proposes a spectral-acceleration-based earthquake intensity measure, which considers the higher modes effect and period elongation effect. A comprehensive study has been carried out to investigate the correlation between structural damages of high-rise chimneys and the proposed intensity measure as well as a number of widely used ground motion parameters under far-field ground motion records. Three RC high-rise chimneys, i.e., a 240 m-high chimney, a 180 m-high chimney, a 120 m-high chimney, are established and analyzed in OpenSees. The structural performance is expressed in terms of Park-Ang damage index, maximum inter-story drift ratio, maximum roof displacement, and maximum floor acceleration. The results indicate that the majority of displacement-related ground motion parameters behave too poor to yield a good correlation with the structural damage index of high-rise chimneys. Moreover, the proposed intensity measure has a high correlation with the structural damage indices, especially with maximum inter-story drift ratio and maximum roof displacement. As a result, the proposed earthquake IM is a promising parameter to predict the structural damage of high-rise chimneys.

### 1. Introduction

An important aspect of seismic risk analysis is the assessment of expected structural damage caused by a specific earthquake ground motion. The ground motion parameters and the structural damage indices are necessary to estimate the structural damage potential of an earthquake. A good correlation of the ground motion parameters and structural damage indices ensures a more accurate evaluation of seismic performance and an effective reduction in the variability of structural response prediction. As a result, the identification of a promising intensity measure, which sufficiently correlates with structural damage indices, is of considerable significance to the seismic risk assessment of the structures.

The high-rise chimneys are tall and long-period structures that will encounter severe structural damage under some earthquakes [1–3]. Wang and Fan [4] investigated failure cases of 739 chimneys and concluded that 19% of them were damaged by earthquakes. The percentage is second only to the damage caused by temperature stress. In 1976, a 180 m RC chimney in Tangshan suffered from an earthquake with magnitude of 7.8 and collapsed at an elevation of 130.5 m due to the 7.1-magnitude aftershock in the same day [4]. In addition, a RC

chimney is damaged during the 2007 Niigata-ken Chuetsu-Oki Earthquake in Japan. This chimney is 60 m high, and the damage was observed at the height of approximately 17.5 m from the ground level, where two layers of longitudinal steel bars were changed to one layer [5]. The failure mechanism of chimneys by earthquake action has been investigated by some researchers[6–8]. In the earthquake, the inertial force is much stronger in horizontal directions, which will result in horizontal displacements at each height of the chimney. The chimney will be damaged when it cannot withstand the horizontal inertial force. In addition, the chimneys could also be seriously damaged by torsional stress as it is reported that the rotational components of ground motion may strongly affect response of tall, slender structures [9,10]. After the Tangshan Earthquake (M 7.8 on July 28, 1976) and the Wenchuan Earthquake (M 8.0 on May 12, 2008) in China, researchers investigated the extent of damage of a few masonry chimneys and reinforced concrete chimneys [11,12]. The results indicate that the presentations of earthquake damage are complex, including horizontal and vertical cracks, inclined cracks, torsion failure and collapse etc.

The degree of the structural damage caused by the earthquakes depends on the seismic performance of the structure and the intensity, energy, and frequency of the ground motions. Previous studies [13–15]

<sup>\*</sup> Corresponding author.

E-mail address: [zhouchangdong@163.com](mailto:zhouchangdong@163.com) (C. Zhou).

<https://doi.org/10.1016/j.soildyn.2020.106282>

Received 25 February 2020; Received in revised form 21 May 2020; Accepted 17 June 2020

Available online 14 July 2020

0267-7261/© 2020 Elsevier Ltd. All rights reserved.

**Table 1**  
Some spectral-acceleration-based intensity measures (IMs).

Period elongation effect	Higher modes effect	
	Power-law form	Linear form
$S^* = S_a(T_1)R_{S_a}^* = S_a(T_1) \frac{S_a(CT_1)^\alpha}{S_a(T_1)^\alpha}$ [32]	$IM_{123} = S_a(T_1)^\alpha S_a(T_2)^\beta S_a(T_3)^\gamma$ [29]	$S_{a12}^* = 0.8S_a(T_1) + 0.2S_a(T_2)$ $S_{a123}^* = 0.8S_a(T_1) + 0.15S_a(T_2) + 0.05S_a(T_3)$ [23]
$IM_{12} = S_a(T_1)^\alpha S_a(2T_1)^\beta$ [29]	$S_{N2} = S_a(T_1)^{0.75} S_a(T_2)^{0.25}$ [26]	$\bar{S}_a^* = \sum_{i=1}^n \alpha_i S_a(T_i)$ $n = \begin{cases} \text{INT}(T_1) & T_1 < 3s \\ 3 & T_1 \geq 3s \end{cases}$ [30]
$S_{N1} = S_a(T_1)^{0.5} S_a(1.5T_1)^{0.5}$ [26]	$S_{12} = S_a(T_1)^{\frac{\alpha_1}{\alpha_1 + \alpha_2}} S_a(T_2)^{\frac{\alpha_2}{\alpha_1 + \alpha_2}}$ $S_{123} = S_a(T_1)^{\frac{\alpha_1}{\alpha_1 + \alpha_2 + \alpha_3}} S_a(T_2)^{\frac{\alpha_2}{\alpha_1 + \alpha_2 + \alpha_3}} S_a(T_3)^{\frac{\alpha_3}{\alpha_1 + \alpha_2 + \alpha_3}}$ [28,31]	
	$\bar{S}_a = \sqrt[n]{\prod_{i=1}^n S_a(T_i)}$ , $n = \begin{cases} 1 & T_1 \leq 1s \\ 0.39T_1 + 1.15 & 1s < T_1 \leq 10s \end{cases}$ [27]	

indicated that the observations of building damages due to the earthquakes had an interdependency between the structural response and the ground motion parameters. As a result, a great number of ground motion parameters have been proposed to represent the structural damage, and the correlation between structural damage and the ground motion parameters has also been widely concerned.

Elenas et al. [16] investigated the correlation between 14 seismic acceleration parameters and the overall structural damage indices (OSDI) of a 7-story RC frame structure and concluded that the first-period spectral acceleration  $S_a(T_1)$  had the strongest correlation with the damage indices. Chen et al. [17] presented a study on the relationship between ground motion parameters and lining damage indices for mountain tunnels. The study clarified that for near-field ground motion without velocity pulses, PGD and PGV were the key parameters, and for far-field ground motions, PGV and Arias intensity were most correlated with lining damage indices. Van Cao et al. [18] investigated the correlation between ground motion parameters of far-field motions and damage indices of a low-rise (3-story) RC frame and concluded that the Velocity spectrum intensity had the best correlation. Wang and Zhao [19] presented a correlation study between structural damage and PGA, PGV, and peak spectrum acceleration (PSA) during the Ms8.0 Wenchuan Earthquake. Kostinakis et al. [20] studied the correlation between ground motion intensity measures and the seismic damage of four medium-rise 3D RC buildings under different directional ground motion input. Kenari et al. [21] examined the correlation between ground motion intensity measures (IM) and seismic damage indices of 4 masonry-infilled steel frames with 3, 5, 8, and 12 stories, respectively. These studies have noted the importance of correlation between ground motion parameters and structural damage indices and concluded that the optimal ground motion parameter, which is most correlated to structural damage, is different due to the structure types. Moreover, most current studies have concerned about this correlation in low-rise buildings and the interdependency between high-rise structures and the ground motion parameters is not straightforward.

Different from the low-rise and medium-rise buildings, the high-rise chimneys are usually tall and soft and possess a large slenderness ratio. Without multi-defense lines for earthquake resistance, this type of structure is prone to undergo severe damage and even collapse under great earthquakes.

This paper presents a correlation study between damage indices of high-rise RC chimneys and ground motion parameters, including a new ground motion intensity measure that considers higher-mode effect and period elongation effect simultaneously. The nonlinear analysis of the 3 RC chimneys structures is carried out in OpenSees.

## 2. Ground motion parameters

Ground motion parameters are essential for describing the

characteristics of strong ground motion in a quantitative and compact form. Due to the complexity of earthquake ground motions, identification of a single parameter that will accurately describe all the significant characteristics is nearly impossible. Therefore, various ground motion parameters have been proposed to characterize the amplitude, frequency content, and duration of strong ground motions.

### 2.1. A new earthquake intensity measure

Previous studies [22–24] have shown that the first-period spectral acceleration  $S_a(T_1)$  is a simple and effective intensity measure for the seismic assessment of some buildings.

However, for high-rise cantilever structures, the dynamic response depends significantly on the higher frequency spectral accelerations in addition to the first-mode spectral acceleration. With the increasing of structural heights, the higher vibration modes will participate in the structural response under earthquake loads. Meanwhile, in the nonlinear stage, the elastic period will be elongated due to the structural stiffness degradation, which is considered closely related to structural damage [25]. To overcome the limitation mentioned above, various modifications have been made to improve  $S_a(T_1)$ , and many spectral-acceleration-based earthquake intensity measures have been recommended [23,26–31]. Some earthquake intensity measures consider the period elongation effect of the structure. These IMs take the power-law form of the fundamental spectral acceleration and spectral acceleration at the elongated period. The elongated period is represented by multiplying elastic first mode period  $T_1$  and a constant  $C$ . Some other IMs account for the higher modes effect. These IMs employ exponential expressions or linear combinations of spectral accelerations. Table 1 summaries some spectral-acceleration-based earthquake intensity measures which consider the period elongation effect or the higher modes effect.

The modified intensity measures in Table 1 either consider the higher modes effect or the period elongation effect at one time. However, the two effects are coupling in the real structural dynamic response. Based on the work of researchers mentioned in Table 1, the new IM is designed to allow for the higher modes effect and period elongation effect at the same time.

The new intensity measure (IM) is expressed as

$$S_c^* = \alpha_1 S_a(T_1)^\beta S_a(CT_1)^{1-\beta} + \sum_{i=2}^n \alpha_i S_a(T_i) \quad (1)$$

Where  $S_a(T_i)$  is the elastic spectral acceleration at the  $i$ th mode,  $n$  is the highest mode that included,  $\alpha_i$  is the  $i$ th modal mass participation factor, and  $\beta$  is the weighting coefficient to adjust the effect of period elongation. Obviously, the  $S_c^*$  is designed to combine the ground motion characteristic and the structural response and meanwhile taking both the higher modes effect and period elongation effect into consideration.

**Table 2**  
Definition of the ground motion parameters.

No.	Ground motion parameter	Definition	Unit
1	First-mode spectral acceleration [23]	$S_a(T_1, \xi = 0.05)$	g
2	Peak ground acceleration (PGA)	$\max a(t) $	g
3	Peak ground velocity (PGV)	$\max v(t) $	cm/sec
4	Peak ground displacement (PGD)	$\max d(t) $	cm
5	PGV/PGA [38]	$\frac{\max v(t) }{\max a(t) }$	sec
6	PGD/PGV [39]	$\frac{\max d(t) }{\max v(t) }$	sec
7	Housner's spectral intensity (SI) [40]	$SI = \int_{0.1}^{2.5} PS_v(T, \xi = 0.05)dT$	cm
8	Acceleration Root-mean-square (RMS) [41]	$a_{rms} = \sqrt{\left(\frac{1}{t_f} \int_0^{tot} a(t)^2 dt\right)}$	g
9	Velocity RMS [41]	$v_{rms} = \sqrt{\left(\frac{1}{t_f} \int_0^{tot} v(t)^2 dt\right)}$	cm/sec
10	Displacement RMS [41]	$d_{rms} = \sqrt{\left(\frac{1}{t_f} \int_0^{tot} d(t)^2 dt\right)}$	cm
11	Significant duration [42]	The significant duration is taken as the interval between the times at which 5% and 95% of the seismic energy is attained	sec
12	Arias intensity (AI) [43]	$AI = \frac{\pi}{2g} \int_0^{tot} a(t)^2 dt$	m/sec
13	Characteristic intensity ( $I_c$ ) [36]	$I_c = a_{rms}^{1.5} \sqrt{t_d}$	-
14	Specific energy density (SED) [36]	$SED = \int_0^{tot} v(t)^2 dt$	-
15	Cumulative absolute velocity (CAV) [36]	$CAV = \int_0^{tot}  a(t)  dt$	cm/sec
16	Cumulative absolute displacement (CAD) [36]	$CAD = \int_0^{tot}  v(t)  dt$	cm
17	Nau and Hall's index ( $E_a$ ) [44]	$E_a = \int_0^{tot} a(t)^2 dt$	-
18	The root-square of $E_a$ ( $A_{rs}$ ) [44]	$A_{rs} = \sqrt{E_a}$	-
19	Nau and Hall's index ( $E_v$ ) [44]	$E_v = \int_0^{tot} v(t)^2 dt$	-
20	The root-square of $E_v$ ( $V_{rs}$ ) [44]	$V_{rs} = \sqrt{E_v}$	-
21	Nau and Hall's index ( $E_d$ ) [44]	$E_d = \int_0^{tot} d(t)^2 dt$	-
22	The root-square of $E_d$ ( $D_{rs}$ ) [44]	$D_{rs} = \sqrt{E_d}$	-
23	Earthquake power index $P_a$ [40]	$P_a = \frac{1}{t_{95} - t_5} \int_{t_5}^{t_{95}} a(t)^2 dt$	g <sup>2</sup>
24	The root-square of $P_a$ ( $a_{RMS}$ ) [37]	$a_{RMS} = \sqrt{P_a}$	g
25	Earthquake power index $P_v$ [40]	$P_v = \frac{1}{t_{95} - t_5} \int_{t_5}^{t_{95}} v(t)^2 dt$	cm <sup>2</sup> /sec <sup>2</sup>
26	The root-square of $P_v$ ( $v_{RMS}$ ) [37]	$v_{RMS} = \sqrt{P_v}$	cm/sec
27	Earthquake power index $P_d$ [40]	$P_d = \frac{1}{t_{95} - t_5} \int_{t_5}^{t_{95}} d(t)^2 dt$	cm <sup>2</sup>
28	The root-square of $P_d$ ( $d_{RMS}$ ) [37]	$d_{RMS} = \sqrt{P_d}$	cm
29	Acceleration spectrum intensity (ASI) [40]	$ASI = \int_{0.1}^{0.5} S_a(T, \xi = 0.05)dT$	cm/sec
30	Velocity spectrum intensity (VSI) [40]	$VSI = \int_{0.1}^{2.5} S_v(T, \xi = 0.05)dT$	cm
31	Effective peak acceleration (EPA) [45]	$EPA = \frac{\text{mean}(S_a^{0.1-0.5}(\xi = 0.05))}{2.5}$	g
32	Effective peak velocity (EPV) [45]	$EPV = \frac{\text{mean}(S_v^{0.1-0.5}(\xi = 0.05))}{2.5}$	cm/sec
33	Riddell's index ( $I_a$ ) [46]	$I_a = \text{PGA} \cdot \sqrt[3]{t_{tot}}$	-
34	Riddell's index ( $I_d$ ) [46]	$I_d = \text{PGD} \cdot \sqrt[5]{t_{tot}}$	-
35	Riddell's index ( $I_v$ ) [46]	$I_v = \sqrt[3]{\text{PGD}^2 \cdot \sqrt[3]{t_{tot}}}$	-
36	Fajfar's index ( $I_f$ ) [47]	$I_f = \text{PGV} \cdot \sqrt[4]{t_{tot}}$	-

Note:  $\xi$  is damping ratio,  $t_{tot}$  is the total duration of the selected ground motion record,  $t_5$  and  $t_{95}$  are time points at which 5% and 95% of the seismic energy is attained.

It should be noted that the  $S_c^*$  possesses very high applicability. More specifically, in the case of  $\beta = 0.5$ , if the higher modes effect is not included, the  $S_c^*$  has the same nature of  $S_{N1}$  and  $S^*$ . Meanwhile, if the period elongation effect is not included (i.e.  $C = 1$ ), the  $S_c^*$  will degenerate into  $\bar{S}_a^*$ . In other words, the  $S_c^*$  unified the period-elongation-effect-involved power-law IMs and linear form IMs together. The proposed IM has been evaluated in the aspect of efficiency and sufficiency in a previous study [33]. In this article, the correlations between  $S_c^*$  and damage indices are investigated and compared with other ground motion parameters.

### 2.2. The other ground motion parameters

To investigate the correlation between the ground motion parameters and the structural damage of high-rise chimneys and make a comparison with the proposed earthquake intensity measure, some seismic ground motion parameters are also selected in this study. These ground motion parameters can be approximately classified into two categories. The first type can be directly extracted from ground motion records, such as peak ground acceleration (PGA), peak ground velocity (PGV), and peak ground displacement (PGD). These parameters have been widely applied in some national design codes due to their convenience and simplicity in usage [34,35]. The second type is indirectly obtained through computer-supported analysis. These parameters include spectral acceleration (SA), effective peak acceleration (EPA), Arias intensity (AI), and Housner's spectral intensity (SI), etc. In this study, 37 ground motion parameters are investigated, and most of them are generally reported by Kramer [36] and Riddell [37]. Table 2 presents the brief definitions and introductions of these parameters.

### 3. Damage indices

Damage indices are straightforward and quantitative tools to assess the damage of structures under earthquakes. Strictly speaking, a damage index is a dimensionless parameter intended to range between 0 for undamaged structural state and 1 for collapse state, with intermediate values representing the degree of structural damage. During an earthquake, the structural damage in reinforced concrete may result from excessive deformations or may be accumulated damage sustained under repeated load reversals. The damage is usually accompanied by structural stiffness degrading effect. A large number of theories and models have been raised for the damage indices [48]. In this study, the local damage index (DI) proposed by Park and Ang [49] is used. The Park-Ang damage index, which is a linear combination of the structural damage caused by excessive deformation and hysteretic energy, has been widely used in earthquake engineering due to the consideration of cumulative damage of structures subjected to repeated cyclic loading. This energy-based damage index is expressed in Eq. [2], where  $u_m$  is the maximum displacement of a structural component under an earthquake action,  $u_u$  is the ultimate displacement subjected to a static monotonic load,  $E_h$  is the hysteretic energy dissipated by the structural component,  $F_y$  is the yield force, and  $\beta$  is a parameter to cover the contribution of cumulative inelastic actions to the structural damage.

$$DI = \frac{u_m}{u_u} + \beta \frac{E_h}{F_y u_u} \quad (2)$$

Apart from the Park-Ang damage index, three damage measures, i.e., maximum inter-story drift (IDR), maximum roof displacement (RD), and the maximum floor acceleration (FA), are also investigated in this article. The maximum inter-story drift  $\theta_{max}$  is an important and practical index to measure structural stiffness and deformation capacity and has

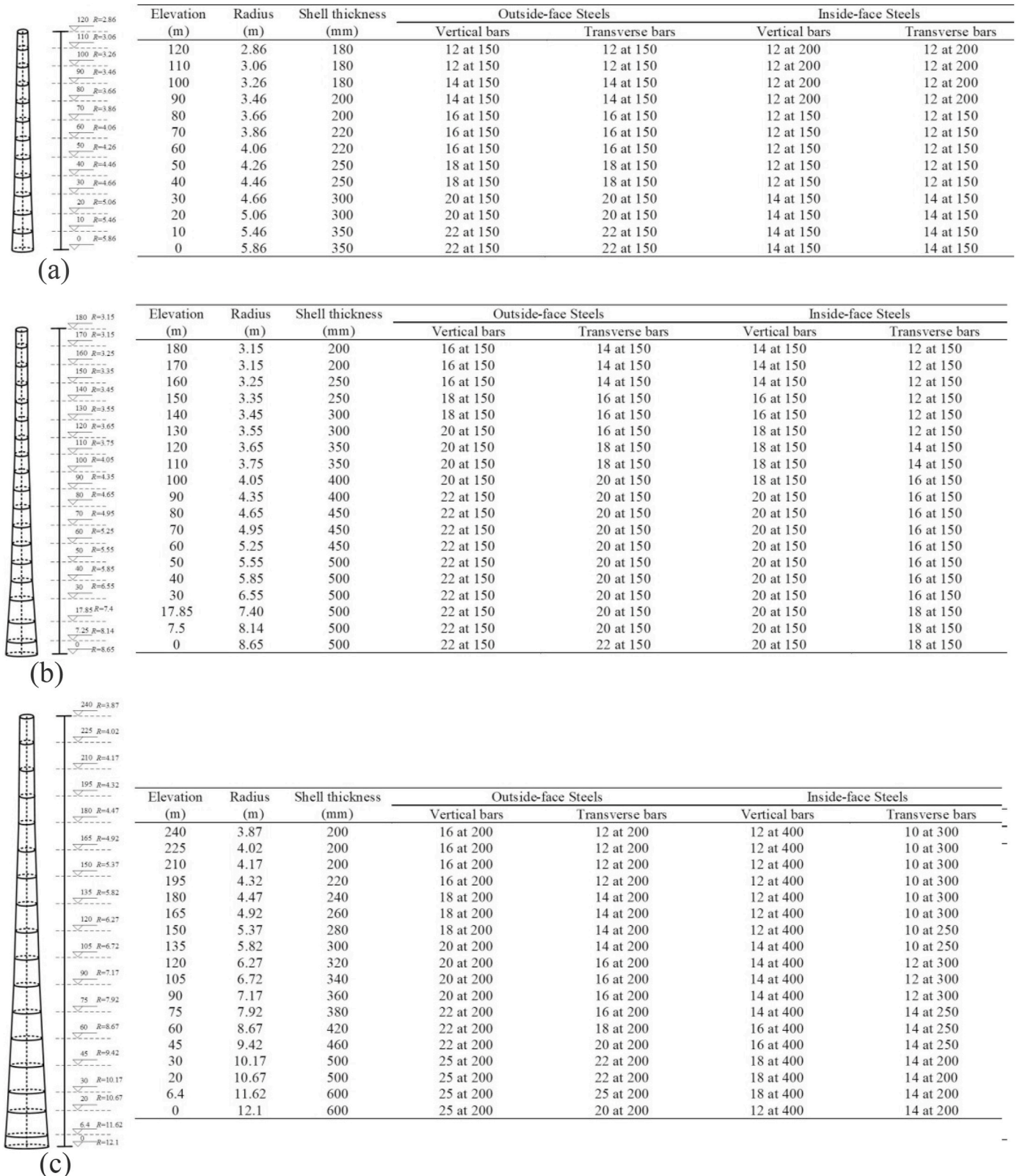


Fig. 1. The characteristics of the RC chimneys, (a) 120 m RC chimney, (b) 180 m RC chimney, (c) 240 m RC chimney.

been widely used in the assessment of various structures. Furthermore, with a large aspect ratio, the high-rise chimneys are dominated by the bending and shear failure under the earthquake loads. The maximum roof displacement can adequately characterize the damage of this type of structure. Furthermore, maximum floor accelerations are essential to

obtain forces for the design of non-structural components and their connections to the primary lateral force resisting system as well as the equipment supported on the floors.

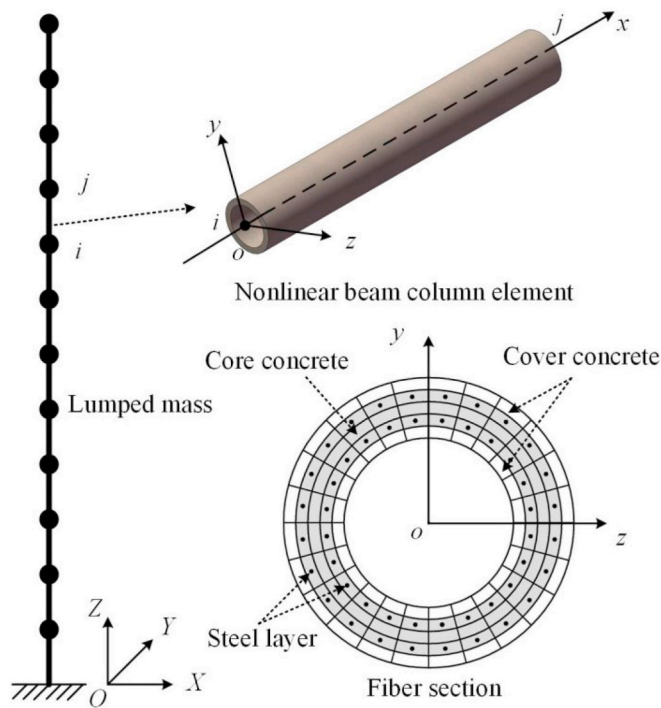
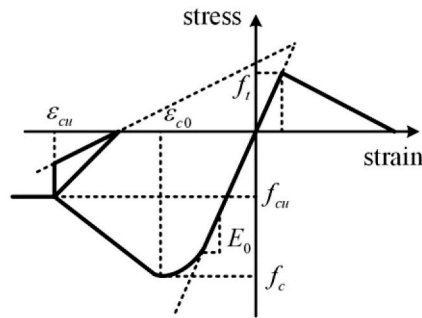
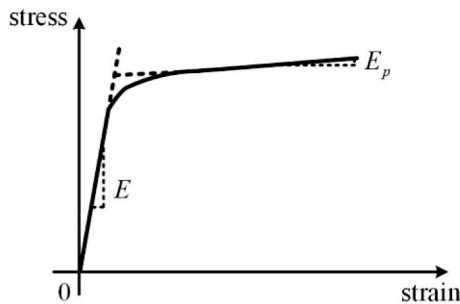


Fig. 2. Finite-element model of the RC chimneys.



(a) strain-stress model of concrete



(b) strain-stress model of steel

Fig. 3. Material models of concrete and steel: (a) strain-stress model of concrete to uniaxial loading in tension and compression, (b) strain-stress model of steel bar.

#### 4. Characteristics of the selected high-rise chimney

In China, a considerable number of high-rise reinforced concrete chimneys in operation were designed and constructed at the end of 20th and the early 21st century to meet the needs of industrial procedures.

The reinforced concrete chimneys, whose typical heights range from 120 m to 300 m, are recognized as high and flexible structures that behave as a vertical cantilever structure fixed as the base. The cross-sections of chimneys are hollow to satisfy industrial procedures, and generally taper varied in height for visually esthetic purposes.

The objective of this study is to evaluate the correlation between the ground motion intensity measures and the response of high-rise RC chimneys, which could represent most of the typologies of existing chimneys in the industrial zone. The heights of the selected three chimneys are 120 m, 180 m, and 240 m. These chimneys were designed according to the chimney code of China [50]. The site soil classification of the regions where the chimneys are located is Class III, which can be classified as the National Earthquake Hazards Reduction Program (NEHRP) site class D (VS,30 in the range of 180 and 360 m/s), and the designed seismic precautionary intensity is Degree 7 associated with design level earthquake of  $PGA = 0.1$  g and maximum considered earthquake of  $PGA = 0.22$  g. The outside diameter of the 240 m chimney varies from 7.74 m at the top to 24.2 m at the base. The bottom radii of the 180 m chimney and the 120 m chimney are 8.65 m and 5.86 m, respectively. The cylinder body of the chimneys is composed of RC shell, heat insulation layer, and the lining. The density of the heat insulation layer and the lining for the 240 m chimney is  $350 \text{ kg/m}^3$  and  $1900 \text{ kg/m}^3$ , respectively. For the 180 m chimney and the 120 m chimney, the density of the heat insulation layer and the lining is  $450 \text{ kg/m}^3$  and  $1200 \text{ kg/m}^3$ . The concrete used in the chimneys is C30, and the steel is HRB335. The longitudinal bars and the circumferential bars are arranged in both sides of the shell. The structural dimensions and reinforcement configuration are illustrated in Fig. 1.

The two-dimensional nonlinear models of the chimneys are developed in the OpenSees platform. The main body is modeled with force-based nonlinear fiber beam-column elements with five integration points along the length. The fiber element assumes that deformations are small and that plane sections remain plane during the loading history. This element is discretized into longitudinal steel and concrete fibers such that the section force-deformation relation is derived by integration of the stress-strain relation of the materials. The fiber element is reliable and computationally efficient in analyzing reinforced concrete members under cyclic loading conditions that induce biaxial bending and axial force, and was proved to be an effective way to capture the dynamic characteristics of the high-rise stack-like structures [22,51]. The structure is modeled using an equivalent lumped mass of each element. The finite-element model of the RC chimneys is presented in Fig. 2.

The numerical model in Fig. 2 has material nonlinearities in the RC shell. The strain-stress relationship is presented in Fig. 3. The uniaxial Kent-Scott-Park constitutive model, which is named Concrete02 model in OpenSees, is used in the concrete. As is shown in Fig. 3(a), this model is characterized as degraded linear unloading/reloading stiffness. In the tensile behavior,  $f_t$  is the tensile strength and the tension softening part is approximated as a linear branch. Moreover,  $f_c$  is the compressive strength of the concrete and  $\epsilon_{c0}$  is the strain at peak strength. The initial elastic modulus is defined as  $E_0 = 2f_c/\epsilon_{c0}$ . After the peak compressive strength, the softening procedure is simplified as a linear function.  $f_{cu}$  is the ultimate compressive strength of the concrete and  $\epsilon_{cu}$  is the corresponding strain. The Steel02 model in OpenSees is used to characterize the behavior of the reinforcement. As is shown in Fig. 3(b), the strain-stress curve is a Menegotto-Pinto model with an isotropic strain hardening effect.  $E$  is the initial elastic modulus of the steel and  $f_y$  is the yield stress. The slope of the plastic branch is  $E_p$ , which can take the value of  $E_p = 0.01E$  according to a previous study [51]. Moreover, the Bauschinger effect is intrinsically incorporated into the material constitutive curve so that the deterioration in the strength of the steel patch could be modeled. The material properties of the concrete and steel in OpenSees are presented in Table 3 and Table 4, respectively.

Rayleigh damping matrix is assumed with the modal damping ratio of 5%. P- $\Delta$  effect is incorporated in the model through the large

**Table 3**  
Property of concrete material modeling.

Material	Model	$E_0$ (N/mm <sup>2</sup> )	$f_t$ (MPa)	$f_c$ (MPa)	$f_{cu}$ (MPa)	$\epsilon_{c0}$	$\epsilon_{c0}$
Concrete	Concrete02	$2.6 \times 10^4$	2.33	-29.4	-5.88	-0.002	-0.0075

**Table 4**  
Property of steel material modeling.

Material	Model	$E$ (N/mm <sup>2</sup> )	$f_y$ (MPa)	$E_p$ (N/mm <sup>2</sup> )
Steel	Steel02	$2.0 \times 10^5$	335	$2.0 \times 10^3$

deformation geometric transformations. The static loads for the chimneys consist of gravity loads of the main RC structures and the additional loads of the heat insulation layer and lining. The weight of the heat insulation layer and the lining is imposed on the structures as uniform load. Table 5 lists the properties of the models of the chimneys. Moreover, the field measurement is also done on the real 240 m chimney [52]. The measured periods are listed to validate the method of establishing the numerical models.

## 5. Selection of ground motions

The structural response may vary significantly in a time-history analysis due to the randomness of the ground motion records. Therefore, the selection of ground motion records is important to minimize the variation and meanwhile maintaining the natural randomness of ground motions. In this study, a total of 44 far-field ground motion records recommended by the FEMA P695 [53] are used to obtain the ground motion parameters in the correlation analysis. The detailed information of ground motion records is listed in Table 6. These far-field records are selected from PEER strong motion database with magnitudes ranging from M6.5 to M7.6. The selected ground motion records are not scaled in the nonlinear analysis. Fig. 4 presents the acceleration spectrum of these records.

## 6. Damage and correlation analysis

Fig. 5 illustrates the Park-Ang damage index distribution of the chimneys along the relative height under San Fernando ground motion record (numbered 41 in Table 3). All the chimneys were elastically designed, and little damaged is observed in Fig. 5. For the 120 m and 180 m chimneys, the maximum damages occur in approximately one-third of the upper part of the structure. In the case of the 240 m chimney, the maximum damage takes place at the bottom of the structure. The structural damage exhibits similar distributions within the one-third of the upper part of all the structures. The inter-story drift ratio (IDR) of the chimneys along relative height under San Fernando ground motion record is shown in Fig. 6. The IDR increases along the relative height of the structures, and the maximum IDR occurs at the top of all the chimneys.

**Table 5**  
Property of the chimneys.

Model	No.	Period (s)	Measured period (s)	Error (%)	Modal mass participation factor $\alpha$	Total mass (kg)
The 240 m chimney	1	3.325	3.413	2.57	0.29	12590225
	2	0.98	1.025	4.39	0.2	
	3	0.45	0.502	10.35	0.12	
The 180 m chimney	1	2.36	–	–	0.422	7047157
	2	0.66	–	–	0.266	
	3	0.27	–	–	0.1	
The 120 m chimney	1	1.92	–	–	0.509	3649853
	2	0.36	–	–	0.27	
	3	0.14	–	–	0.139	

To evaluate the grade of the interrelation between ground motion parameters and the damage indices quantitatively, the correlation coefficient after Pearson has been calculated. In statistics, the Pearson correlation coefficient, which is defined as the covariance of the two variables divided by the product of their standard deviations, is a measure of the linear correlation between two variables  $X$  and  $Y$ . The Pearson correlation coefficient is given by the relation:

$$\rho_{\text{Pearson}} = \frac{\sum_{i=1}^n (X_i - \bar{X})(Y_i - \bar{Y})}{\sqrt{\sum_{i=1}^n (X_i - \bar{X})^2 \sum_{i=1}^n (Y_i - \bar{Y})^2}} \quad (3)$$

where  $\bar{X}$  and  $\bar{Y}$  are the mean value of  $X_i$  and  $Y_i$  data, respectively.  $n$  is the number of pairs of values in the data.

### 6.1. Correlation study of the proposed intensity measure

Due to the cumulation of the structural damage during the dynamic response, period elongation effect can be significant for higher excitation levels. The elongated period in the proposed IM  $S_c^*$  is simplified as the product of the first period  $T_1$  and the period elongation coefficient  $C$ . Several period elongation coefficients have been proposed previously in terms of the efficiency of different ground motion intensity measures for different types of structures. Lin et al. [26] and Cordova et al. [32] proposed that the best period elongation coefficients for RC frame structures were 1.5 and 2.0, respectively. To obtain the proper period elongation coefficient in  $S_c^*$ , the Pearson correlation coefficient of the DI and the  $S_c^*$  with different  $C$ s is investigated.

Fig. 7 presents the relationship between the period elongation coefficient  $C$  and the Pearson correlation coefficient, which is obtained through regression analysis between the Park-Ang DI and the  $S_c^*$ . For all the structures,  $C$  takes the value of  $C = 1$  (no elongation),  $C = 1.2$ ,  $C = 1.5$  [26],  $C = 1.8$ ,  $C = 2.0$  [32],  $C = 2.2$ . For all the chimneys, the variation of the Pearson correlation coefficient follows a similar pattern. As the period elongation coefficient rises from 1 to 2.2, the Pearson correlation coefficient between DI and the  $S_c^*$  first increases and then decreases. In all the cases, the optimum coefficient value is 1.2, which is smaller compared with the suggestions for low-rise RC frame structures. It can be concluded that even though the existed chimney is designed to resist the earthquake during the elastic stage, the period elongation effect, which is due to the cumulation of structural damage in the dynamic response, is still observed. However, the structural damage in the chimneys is less remarkable compared with the RC frame structures as they are designed conservatively.

The scatter plots of  $S_a(T_1) - \text{DI}$  and  $S_c^* - \text{DI}$  for the ground motion

**Table 6**  
Information of the earthquake ground motion records.

ID No.	File names	Station	M	R (km)	PGA (g)	PGV (m/s)	PGD (m)
1	NORTHR/MUL009	Beverly Hills – Mulhol	6.7	17.15	0.42	0.59	0.13
2	NORTHR/MUL279	Beverly Hills – Mulhol	6.7	17.15	0.4879	0.67	0.1217
3	NORTHR/LOS000	Canyon Country-WLC	6.7	12.44	0.41	0.43	0.12
4	NORTHR/LOS270	Canyon Country-WLC	6.7	12.44	0.4716	0.41	0.1457
5	DUZCE/BOL000	Bolu	7.1	12.04	0.73	0.56	0.23
6	DUZCE/BOL090	Bolu	7.1	12.04	0.8057	0.66	0.1309
7	HECTOR/HEC000	Hector	7.1	11.66	0.27	0.29	0.23
8	HECTOR/HEC090	Hector	7.1	11.66	0.3282	0.45	0.1069
9	IMPVALL/H-DLT262	Delta	6.5	22.03	0.24	0.26	0.12
10	IMPVALL/H-DLT352	Delta	6.5	22.03	0.35	0.33	0.16
11	IMPVALL/H-E11140	El Centro Array #11	6.5	12.56	0.36	0.34	0.16
12	IMPVALL/H-E11230	El Centro Array #11	6.5	12.56	0.38	0.45	0.21
13	KOBE/NIS000	Nishi-Akashi	6.9	7.08	0.51	0.37	0.1
14	KOBE/NIS090	Nishi-Akashi	6.9	7.08	0.46	0.38	0.12
15	KOBE/SHI000	Shin-Osaka	6.9	19.15	0.24	0.38	0.09
16	KOBE/SHI090	Shin-Osaka	6.9	19.15	0.23	0.22	0.10
17	KOCAELI/DZC180	Duzce	7.5	15.37	0.31	0.59	0.44
18	KOCAELI/DZC270	Duzce	7.5	15.37	0.36	0.56	0.25
19	KOCAELI/ARC000	Arcelik	7.5	13.49	0.22	0.18	0.14
20	KOCAELI/ARC090	Arcelik	7.5	13.49	0.13	0.40	0.32
21	LANDERS/YER270	Yermo Fire Station	7.3	23.62	0.25	0.51	0.44
22	LANDERS/YER360	Yermo Fire Station	7.3	23.62	0.15	0.29	0.23
23	LANDERS/CLW-LN	Coolwater	7.3	19.74	0.28	0.26	0.14
24	LANDERS/CLW-TR	Coolwater	7.3	19.74	0.42	0.43	0.15
25	LOMAP/CAP000	Capitola	6.9	15.23	0.53	0.35	0.09
26	LOMAP/CAP090	Capitola	6.9	15.23	0.44	0.30	0.05
27	LOMAP/G03000	Gilroy Array #3	6.9	12.82	0.56	0.36	0.08
28	LOMAP/G03090	Gilroy Array #3	6.9	12.82	0.37	0.45	0.24
29	MANJIL/ABBAR-L	Abbar	7.4	12.55	0.52	0.42	0.15
30	MANJIL/ABBAR-T	Abbar	7.4	12.55	0.50	0.51	0.24
31	SUPERST/B-ICC000	El Centro Imp. Co.	6.5	18.2	0.36	0.46	0.18
32	SUPERST/B-ICC090	El Centro Imp. Co.	6.5	18.2	0.26	0.41	0.22
33	SUPERST/B-POE270	Poe Road (temp)	6.5	11.16	0.48	0.41	0.08
34	SUPERST/B-POE360	Poe Road (temp)	6.5	11.16	0.29	0.29	0.11
35	CAPEMEND/RIO270	Rio Dell Overpass	7	14.3	0.39	0.44	0.22
36	CAPEMEND/RIO360	Rio Dell Overpass	7	14.3	0.55	0.32	0.41
37	CHICHI/CHY101-E	CHY101	7.6	9.94	0.35	0.51	0.35
38	CHICHI/CHY101-N	CHY101	7.6	9.94	0.40	1.09	0.74
39	CHICHI/TCU045-E	TCU045	7.6	26	0.47	0.50	0.39
40	CHICHI/TCU045-N	TCU045	7.6	26	0.51	0.46	0.15
41	SFERN/PEL090	LA – Hollywood Stor	6.6	22.77	0.21	0.19	0.12
42	SFERN/PEL180	LA – Hollywood Stor	6.6	22.77	0.22	0.21	0.16
43	FRIULI/A-TMZ000	Tolmezzo	6.5	15.82	0.35	0.22	0.04
44	FRIULI/A-TMZ270	Tolmezzo	6.5	15.82	0.31	0.30	0.05

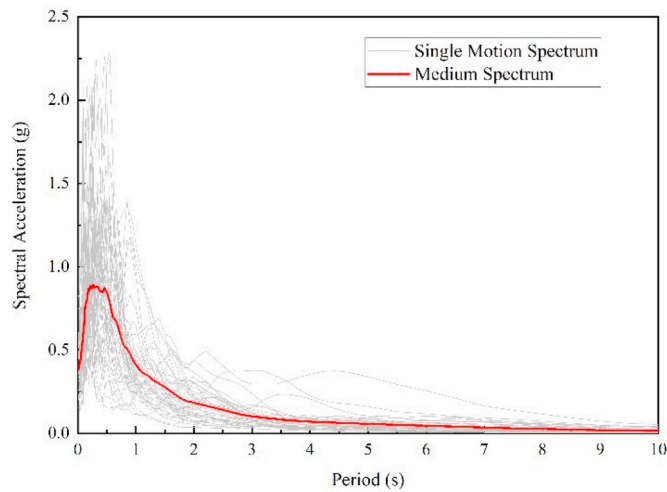


Fig. 4. Acceleration spectrum of the ground motion records.

records are presented in Fig. 8. The proposed  $S_c^*$  is modified from  $S_a(T_1)$  with higher modes effect and period elongation effect participated simultaneously. According to the previous conclusions, the number of

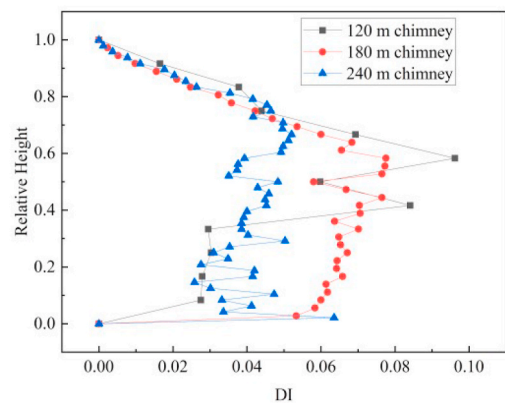


Fig. 5. Park-Ang damage index distribution of the chimneys along the relative height.

modes participated in  $S_c^*$  for the 120 m, 180 m, and 240 m chimneys are 1, 2, and 2, respectively. Compared with  $S_a(T_1)$ , the correlation coefficients of  $S_c^*$  are improved in the three chimneys. For the 120 m chimney, the Pearson correlation coefficient increases from 0.7597 to 0.7712. As there is only one mode in this case, the increment in Pearson

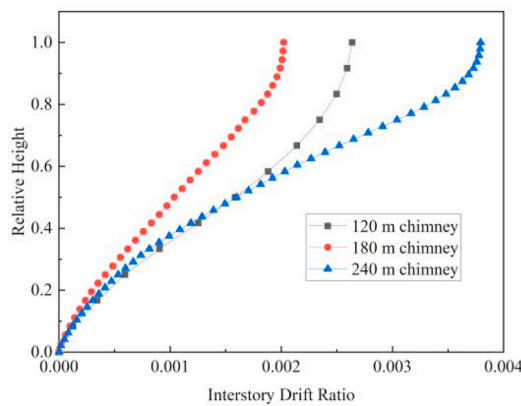


Fig. 6. The inter-story drift ratio of the chimneys along the relative height.

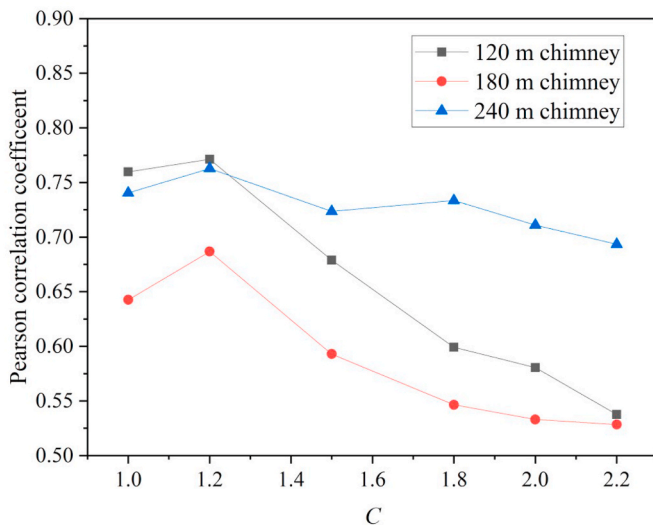


Fig. 7. Comparison between different elongation coefficients for the chimneys.

correlation coefficient indicates the consideration of period elongation effect is essential. For the 180 m chimney, the Pearson correlation coefficient rises from 0.6198 to 0.6868. The most significant growth of the correlation coefficient is in the 240 m chimney case, where  $\rho_{\text{Pearson}}$  increases from 0.3193 to 0.7628. As the height of the structure increases, more vibration modes will be involved in the dynamic response of the structure. In the last cases,  $S_c^*$  is improved from  $S_a(T_1)$  with two modes and  $C = 1.2$  included. As the structural height rises from 180 m to 240 m, a more considerable increase in correlation coefficient is observed, which indicates the necessity to consider higher modes effect and period elongation effect simultaneously in the earthquake intensity measures in high-rise chimneys.

The linear correlation coefficients after Pearson between the 37 ground motion parameters and the Park-Ang damage index (DI) are presented in Fig. 9. For the 120 m chimney, the velocity spectrum intensity (VSI) has the highest correlation with the DI among other parameters with the effective peak velocity (EPV) and Housner's spectral intensity (SI) following behind, which is consistent with the conclusions from Cao and Ronagh [18]. The proposed  $S_c^*$  ranks the fourth with a slight advantage over the  $S_a(T_1)$ . For the 180 m chimney, the Housner's spectral intensity (SI) is the most efficient ground motion parameter. The next two candidates are velocity spectrum intensity (VSI) and effective peak velocity (EPV), as can be seen from the results shown in Fig. 9(b). As for the  $S_c^*$ , the position remains the same as 120 m chimney case. In the case of the 240 m chimney, the top four ground motion

parameters are VSI, EPV, SI, and  $S_c^*$ , which is entirely consistent with the situation in the 120 m chimney. Overall, some velocity-related ground motion parameters (VSI, EPV, SI, PGV, Velocity RMS) demonstrate a robust correlation with the DI of the chimneys. On the contrary, almost all the displacement-related ground motion parameters (PGD, Displacement RMS, CAD,  $E_d$ ,  $D_{rs}$ ,  $P_d$ ,  $d_{RMS}$ ,  $I_d$ ) exhibit weak correlation with the damage index as such are not reasonable to be selected to represent the intensity of a ground motion record. Similarly, the significant duration is poorly related to the structural damage in all the cases, with the correlation coefficient less than 0.1. Moreover, although the PGV/PGA and PGD/PGV both reflect some period content of the earthquake ground motions, the correlations between the parameters and the DI are quite different. In the compound intensity measures ( $I_a$ ,  $I_d$ ,  $I_v$ ,  $I_j$ ), the rankings, in descending order, are  $I_a$ ,  $I_f$ ,  $I_v$  and  $I_d$ .

The best correlation of the VSI or SI in the chimneys can be explained by their advanced definition, where a wide range of frequency content and velocity are taken into consideration. Generally, the velocity-related ground motion parameters seem to be related to both structural force (acceleration) and deformation (displacement), which in turn govern the Park-Ang damage of the chimneys. Moreover, it should be noted that the conventionally used parameters PGA and  $S_a(T_1)$  have limitations in representing the damage potential of high-rise chimneys under the far-field ground motions.

Fig. 10 and Fig. 11 illustrate the linear correlation coefficient after Pearson between the ground motion parameters and the maximum inter-story drift ratio (IDR) and the maximum roof displacement (RD). It is worth pointing that the proposed  $S_c^*$  possesses the best correlation with displacement-based damage measures among other ground motion parameters, as shown in Fig. 10(b), (c), Fig. 11(a), (b), and 11(c). In Fig. 10 (a), the  $S_c^*$  ranks the second place with a minimal disadvantage. This indicates that the modification from the  $S_a(T_1)$  with period elongation effect included is very effective and essential in terms of displacement-based structural response. From this point of view, the proposed earthquake intensity measure is a very promising parameter in representing the displacement-based damage potential of high-rise chimneys under the far-field ground motions. From these figures, it can also be concluded that for the velocity-related ground motion parameters, especially VSI, SI, and EPV, the correlation with the structural damage state remains strong when the damage measure based on displacement demands (maximum IDR and maximum RD).

Although the maximum IDR and maximum RD belong to the displacement demands, the comparison between Figs. 10 and 11 does not reveal a severe trend, see for example that  $I_a$  is more correlated to maximum IDR than  $I_d$  in Fig. 10. However, the situation reverses in Fig. 11. This may due to the interdependency between the parameters and damage measures depends on both earthquake intensity measure as well as on the structural characteristics.

Fig. 12 depicts the linear correlation coefficient after Pearson between the ground motion parameters and the maximum floor acceleration (FA). Compared with Figs. 9–11, the most significant difference is the growth of acceleration-related ground motion parameters (PGA, Acceleration RMS,  $E_a$ ,  $A_{rs}$ ,  $P_a$ ,  $a_{RMS}$ , ASI,  $I_a$ ) in the correlation coefficient. For example, the ranking orders of PGA in Fig. 12(a), (b), and (c) are 4th, 4th, and 1st, which have made quite significant progress compared with other cases. This is reasonable as the maximum floor acceleration could be considered as the direct magnification of the PGA [54]. Consequently, the maximum floor acceleration is sensitive to the acceleration-related ground motion parameters, thereby resulting in a growth in correlation. Furthermore, the VSI, SI, and EPV maintain a high level of correlation with the maximum RD.

To sum up, despite the fact that the different damage measures are used in the correlation study, there are still several conclusions in common. First, the VSI, SI, and EPV have very strong correlations with the structural damage for the high-rise chimneys. Among the majority ground motion parameters, the VSI and SI are superior definitions for

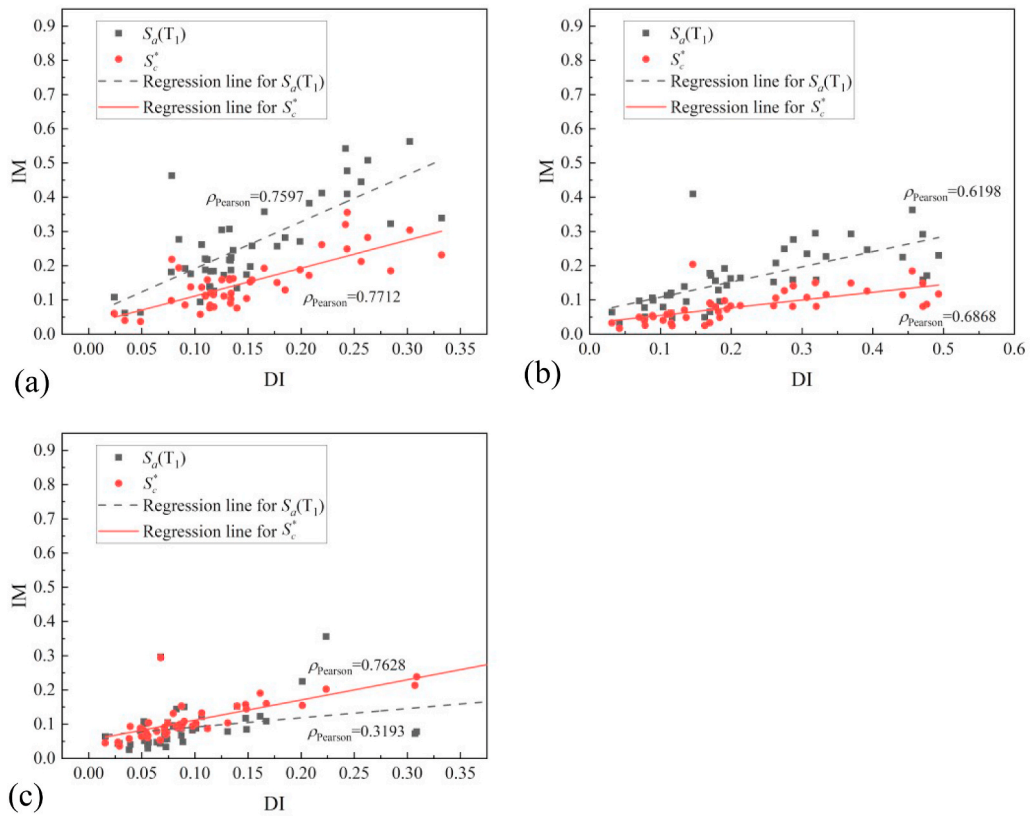


Fig. 8. The regression scatter plots of the chimneys: (a) 120 m chimney, (b) 180 m chimney, (c) 240 m chimney.6.2. Correlation between ground motion parameters and structural response.

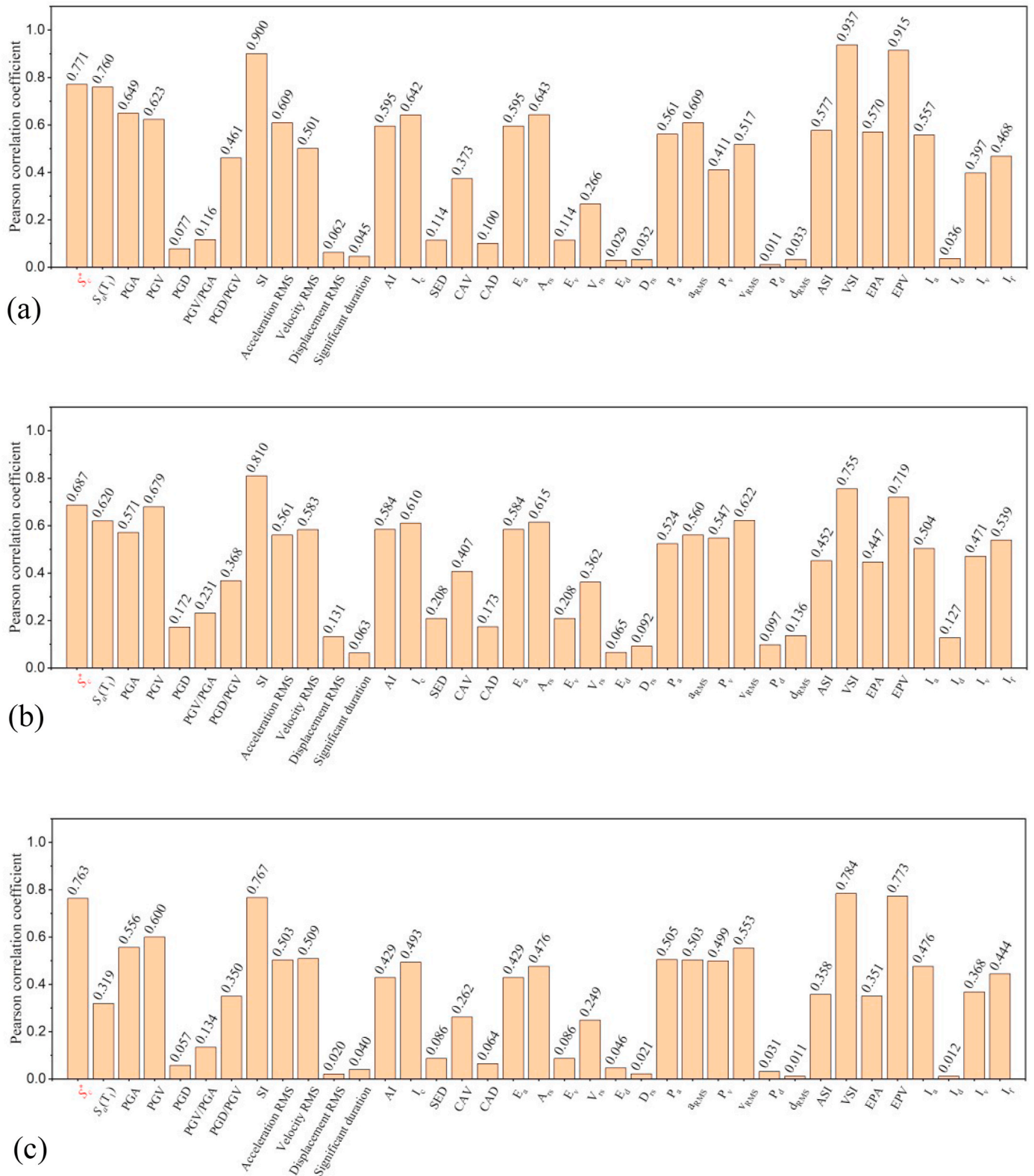


Fig. 9. Pearson correlation coefficients between DI and the ground motion parameters: (a) 120 m chimney, (b) 180 m chimney, (c) 240 m chimney.

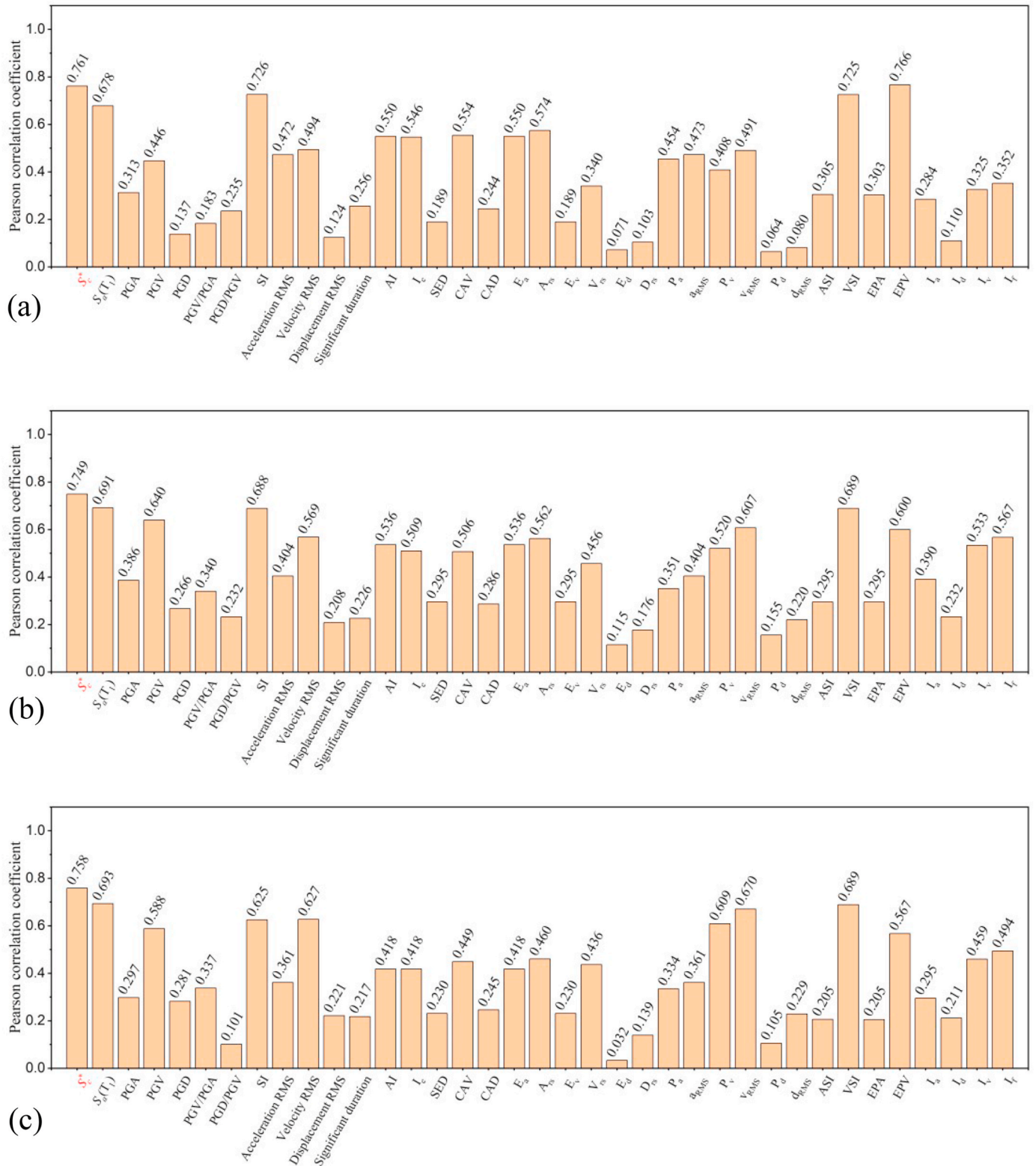


Fig. 10. Pearson correlation coefficients between maximum inter-story drift ratio (IDR) and the ground motion parameters: (a) 120 m chimney, (b) 180 m chimney, (c) 240 m chimney.

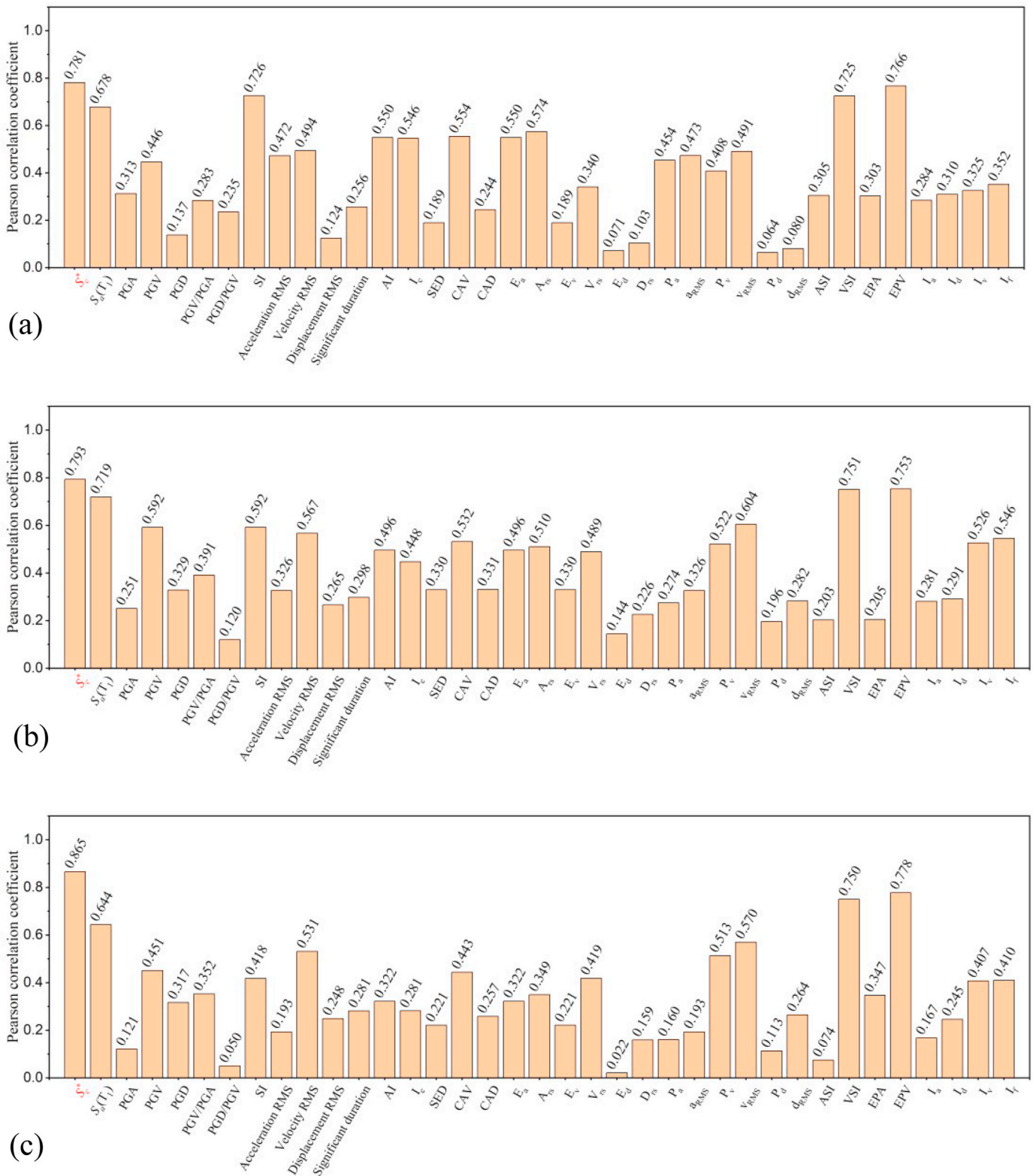


Fig. 11. Pearson correlation coefficients between maximum roof displacement (RD) and the ground motion parameters: (a) 120 m chimney, (b) 180 m chimney, (c) 240 m chimney.

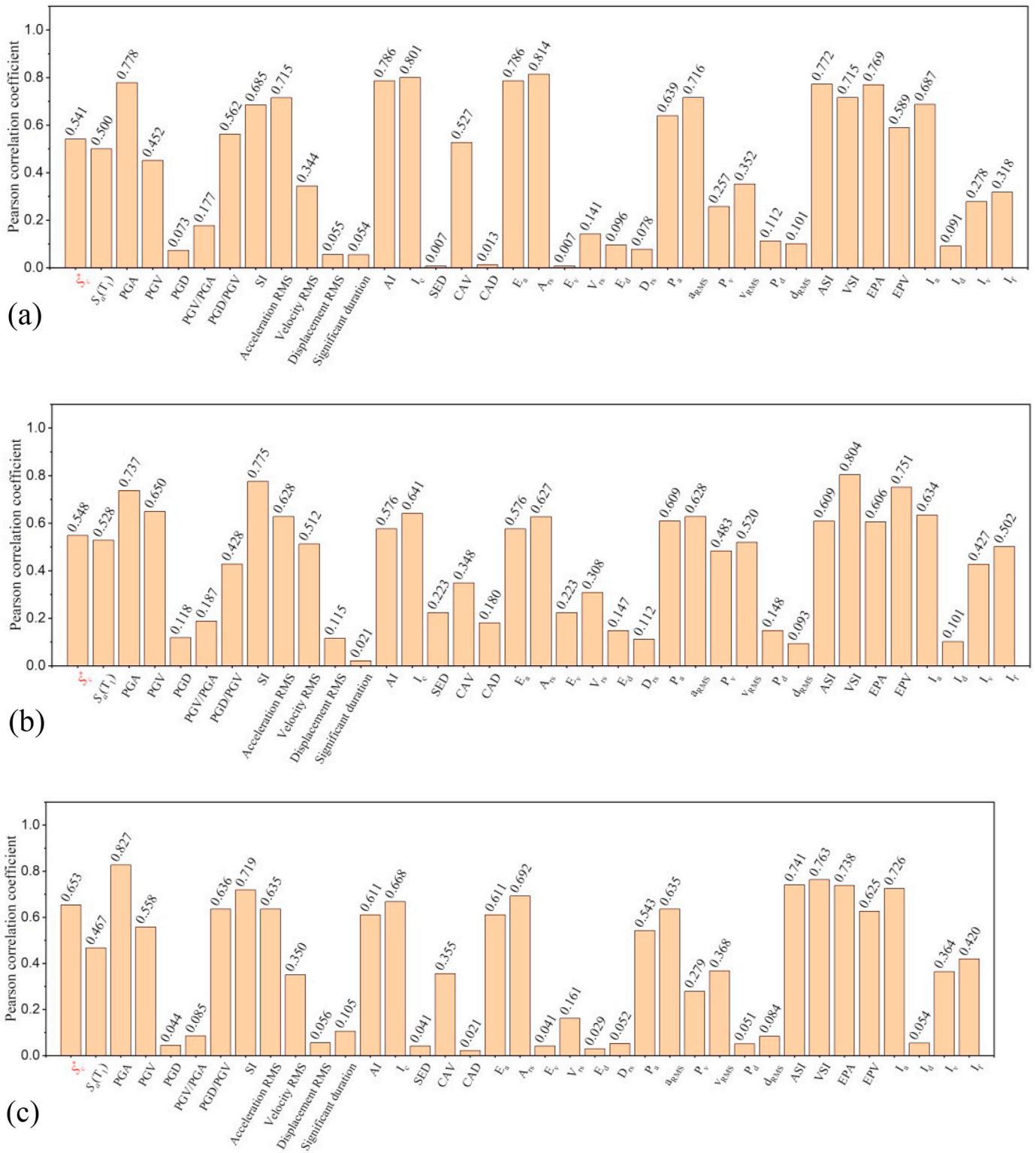


Fig. 12. Pearson correlation coefficients between maximum roof acceleration.

**Table 7**  
Correlation among structural damage measures of the chimneys.

	Damage measures	max DI	max IDR	max RD	max FA
120 m chimney	max DI	1	0.77723	0.7311	0.76243
	max IDR		1	0.99517	0.66563
	max RD			1	0.6423
	max FA				1
180 m chimney	max DI	1	0.92994	0.83435	0.85388
	max IDR		1	0.97405	0.4858
	max RD			1	0.34058
	max FA				1
240 m chimney	max DI	1	0.86795	0.73734	0.76402
	max IDR		1	0.96852	0.57168
	max RD			1	0.4259
	max FA				1

the intensity of ground motion than any other parameters. Second, the displacement-related ground motion parameters (PGD, Displacement RMS, CAD,  $E_d$ ,  $D_{RS}$ ,  $P_d$ ,  $d_{RMS}$ ,  $I_d$ ) generally exhibit weak correlation with the structural damage of the high-rise chimneys. These ground motion parameters are not reprehensible of the potential structural damage. Last but not least, the  $S_c^*$  shows stronger correlation with the damage measures than  $S_a(T_1)$ , which indicates that the incorporation of higher modes effect and period elongation effect is significant and essential, especially in the correlation study between displacement-based damages.

## 6.2. Correlation between damage measures

To investigate the correlation between the maximum Park-Ang damage index and the maximum IDR, maximum RD, and maximum RA, the Pearson's correlation coefficients are evaluated and shown in Table 7. In all the structures, the max IDR has the highest correlation with max DI, with max FA and max RD following behind. Furthermore, the max IDR and max RD show robust correlations between each other. This can be attributed to the dependence on similar structural displacement demand.

## 7. Conclusions

In this paper, a spectral-acceleration-based combination-type earthquake intensity measure is presented. The correlation between damage measures and 37 ground motion parameters as well as the correlation between Park-Ang damage index and maximum inter-story drift ratio, maximum roof displacement, and maximum floor acceleration are investigated under 44 far-field ground motions. The comparative assessment of the results has led to the following conclusions:

- For all the three chimneys, the correlation study between the proposed  $S_c^*$  and Park-Ang damage index indicates that the period elongation effect is noticeable. The period elongation coefficient for high-rise chimneys is proposed to be 1.2 in  $S_c^*$ .
- In the cases of the 180 m chimney and the 240 m chimney, the proposed  $S_c^*$  has the best correlation with the maximum IDR and the maximum RD. In addition, this study reaffirms the superiority of VSI in representing the potential damage of structures. Both the two parameters could be used to assess the damage potential of the existing RC chimneys.
- Although the code for chimneys in China still uses PGA for design purposes, this study shows that PGA has limitations in representing the maximum Park-Ang DI, maximum IDR, and maximum RD of high-rise chimneys under the far-field ground motions.

## Declaration of competing interest

The authors declare that they have no known competing financial interests or personal relationships that could have appeared to influence the work reported in this paper.

## CRediT authorship contribution statement

**Yikun Qiu:** Conceptualization, Methodology, Software. **Changdong Zhou:** Supervision, Validation. **Siha A:** Writing - review & editing.

## Acknowledgment

The authors are grateful to the support from the National Natural Science Foundation of China under the contract of 51678039, 51478033.

## References

- Huang W, Gould PL, Martinez R, Johnson GS. Non-linear analysis of a collapsed reinforced concrete chimney. *Earthquake Eng Struct* 2004;33(4):485–98.
- Wilson JL. Earthquake response of tall reinforced concrete chimneys. *Eng Struct* 2003;25(1):11–24.
- Zhou C, Tian M, Guo K. Seismic partitioned fragility analysis for high-rise RC chimney considering multidimensional ground motion. *Struct Des Tall Spec* 2019;28(1):e1568.
- Wang L, Fan XY. Failure cases of high chimneys: a review. *Eng Fail Anal* 2019;105:1107–17.
- Kim Suhee, Hitoshi S. Dynamic response analysis of a tall RC chimney damaged during 2007 Niigata-ken Chuetsu-Oki Earthquake. In: Proc15th world conference on earthquake engineering; september; 2012. Lisbon2012.
- Ghobarah A, Bamber T. Seismic response and retrofit of industrial brick masonry chimneys. *Can J Civ Eng* 1992;19(1):117–28.
- Longarini N, Zucca M. A chimney's seismic assessment by a tuned mass damper. *Eng Struct* 2014;79:290–6.
- Minghini F, Milani G, Tralli A. Seismic risk assessment of a 50 m high masonry chimney using advanced analysis techniques. *Eng Struct* 2014;69:255–70.
- Igel H, Brokesova J, Evans J, Zembaty Z. Preface to the special issue on "Advances in rotational seismology: instrumentation, theory, observations, and engineering. *J Seismol* 2012;16(4):571–2.
- Lee WHK, Celebi M, Todorovska MI, Igel H. Introduction to the special issue on rotational seismology and engineering applications. *Bull Seismol Soc Am* 2009;99(2b):945–57.
- Wenzao S, Yadi Y. The damage law and analysis of chimney. *World Earthq Eng* 1988;3:34–9 (in Chinese).
- CAoB Research. Photo collection of 2008 wenchuan earthquake damage to buildings. Beijing, China: China Architecture & Building Press; 2008.
- Elenas A. Interdependency between seismic acceleration parameters and the behaviour of structures. *Soil Dynam Earthq Eng* 1997;16(5):317–22.
- Elenas A. Correlation between seismic acceleration parameters and overall structural damage indices of buildings. *Soil Dynam Earthq Eng* 2000;20(1-4):93–100.
- Perrault M, Gueguen P. Correlation between ground motion and building response using California earthquake records. *Earthq Spectra* 2015;31(4):2027–46.
- Elenas A, Meskouris K. Correlation study between seismic acceleration parameters and damage indices of structures. *Eng Struct* 2001;23(6):698–704.
- Chen ZY, Wei JS. Correlation between ground motion parameters and lining damage indices for mountain tunnels. *Nat Hazards* 2013;65(3):1683–702.
- Van Cao V, Ronagh HR. Correlation between seismic parameters of far-fault motions and damage indices of low-rise reinforced concrete frames. *Soil Dynam Earthq Eng* 2014;66:102–12.
- Wang ZJ, Zhao BM. Correlations between structural damage and ground motion parameters during the Ms8.0 Wenchuan Earthquake. *Soil Dynam Earthq Eng* 2015;72:129–37.
- Kostinakis K, Athanopoulou A, Morfidis K. Correlation between ground motion intensity measures and seismic damage of 3D R/C buildings. *Eng Struct* 2015;82:151–67.
- Kenari MS, Celikag M. Correlation of ground motion intensity measures and seismic damage indices of masonry-infilled steel frames. *Arabian J Sci Eng* 2019;44(5):5131–50.
- Asgarian B, Mirtaheeri MYM, Samani HR, Alanjari P. Incremental dynamic analysis of high-rise towers. *Struct Des Tall Spec* 2010;19(8):922–34.
- Shome N. Probabilistic seismic demand analysis of nonlinear structures. Stanford University; 1999.
- Shome N, Cornell CA, Bazzurro P, Carballo JE. Earthquakes, records, and nonlinear responses. *Earthq Spectra* 1998;14(3):469–500.
- Kadas K, Yakut A, Kazaz I. Spectral ground motion intensity based on capacity and period elongation. *J Struct Eng* 2011;137(3):401–9.

- [26] Lin L, Naumoski N, Saatcioglu M, Foo S. Improved intensity measures for probabilistic seismic demand analysis. Part 1: development of improved intensity measures. *Can J Civ Eng* 2010;38(1):79–88.
- [27] Lu X, Ye LP, Lu XZ, Li MK, Ma XW. An improved ground motion intensity measure for super high-rise buildings. *Sci China Technol Sci* 2013;56(6):1525–33.
- [28] Su NF, Lu XL, Zhou Y, Yang TY. Estimating the peak structural response of high-rise structures using spectral value-based intensity measures. *Struct Des Tall Spec* 2017; 26(8).
- [29] Vamvatsikos D, Cornell CA. Developing efficient scalar and vector intensity measures for IDA capacity estimation by incorporating elastic spectral shape information. *Earthquake Eng Struct* 2005;34(13):1573–600.
- [30] Zhang YT, He Z, Lu WG, Yang YF. A spectral-acceleration-based linear combination-type earthquake intensity measure for high-rise buildings. *J Earthq Eng* 2018;22(8):1479–508.
- [31] Zhou Y, Su N, Lu X. Study on intensity measure of incremental dynamic analysis for high-rise structures. *Jianzhu Jiegou Xuebao J Build Struct* 2013;34(2):53–60.
- [32] Cordova PP, Deierlein GG, Mehanny SSF, Cornell CA, editors. Development of a two-parameter seismic intensity measure and probabilistic assessment procedure. The second US-Japan workshop on performance-based earthquake engineering methodology for reinforced concrete building structures. Japan: Sapporo; 2001.
- [33] Qiu YK, Zhou C, S A, Zhang G. A spectral-acceleration-based combination-type earthquake intensity measure for high-rise stack-like structures. *Advances in Structural Engineering* 2020;23(7):1350–66. <https://doi.org/10.1177/1369433219894237>.
- [34] TBCo Japan. The building standard law of Japan. Japan: The Building Centre of Japan; 2000.
- [35] MOC. Code for seismic design of buildings gb50011-2010. Beijing, China: Ministry of Construction of the People's Republic of China; 2010.
- [36] Kramer SL. Geotechnical earthquake engineering. Englewood Cliffs: Prentice Hall; 1996.
- [37] Riddell R. On ground motion intensity indices. *Earthq Spectra* 2007;23(1):147–73.
- [38] Tso WK, Zhu TJ, Heidebrecht AC. Engineering implication of ground motion A/V ratio. *Soil Dynam Earthq Eng* 1992;11(3):133–44.
- [39] Bommer JJ, Elnashai AS, Weir AG. Compatible acceleration and displacement spectra for seismic design codes. Proceedings of the 12th world conference on earthquake engineering; 1 January–4 February; auckland, New Zealand 2000.
- [40] Housner GW, Martel RR, Alford JL. Spectrum analysis of strong-motion earthquakes. *Bull Seismol Soc Am* 1953;43(2):97–119.
- [41] Dobry R, Idriss IM, Ng E. Duration characteristics of horizontal components of strong-motion earthquake records. *Bull Seismol Soc Am* 1978;68(5):1487–520.
- [42] Bommer JJ, Martinez-Pereira A. The effective duration of earthquake strong motion. *J Earthq Eng* 1999;3(2):127–72.
- [43] Arias A. Measure of earthquake intensity of Seismic Design for Nuclear Power Plants/Hansen. In: Robert J, editor. Cambridge. Mass Massachusetts Inst of Tech Press; 1970. p. 438–83. 1970:Medium: X.
- [44] Nau JM, Hall WJ. Scaling methods for earthquake response spectra. *J Struct Eng Asce* 1984;110(7):1533–48.
- [45] ATC. Tentative provisions for the development of seismic regulations for buildings, ATC 3–06. Redwood City, CA 1978.
- [46] Riddell R, Garcia JE. Hysteretic energy spectrum and damage control. *Earthquake Eng Struct* 2001;30(12):1791–816.
- [47] Fajfar P, Vidic T, Fischinger M. A measure of earthquake motion capacity to damage medium-period structures\*. *Soil Dynam Earthq Eng* 1990;9(5):236–42.
- [48] Williams MS, Sexsmith RG. Seismic damage indices for concrete structures: a state-of-the-art review. *Earthq Spectra* 1995;11(2):319–49.
- [49] Park YJ, Ang AHS. Mechanistic seismic damage model for reinforced-concrete. *J Struct Eng Asce* 1985;111(4):722–39.
- [50] CMO Construction. Code for seismic design of building (GB 50011-1989). Beijing, China: China Architecture & Building Press; 1989.
- [51] Zhou CD, Zeng XL, Pan QL, Liu B. Seismic fragility assessment of a tall reinforced concrete chimney. *Struct Des Tall Spec* 2015;24(6):440–60.
- [52] Zeng X. Study on seismic performance of high-rise reinforced concrete chimney structure [Master Thesis]. Beijing Jiaotong University; 2014.
- [53] FEMA FEMA. P695: quantification of building seismic performance factors. Redwood City, CA, USA: Applied Technology Council; 2009.
- [54] Rodriguez ME, Restrepo JI, Carr AJ. Earthquake-induced floor horizontal accelerations in buildings. *Earthquake Eng Struct* 2002;31(3):693–718.